Injection locking and polarization switching bistability in a 1550nm-VCSEL subject to parallel optical injection

Florian Denis-le Coarer, Ana Quirce, Pablo Pérez, Angel Valle, Luis Pesquera, Marc Sciamanna, Hugo Thienpont, and Krassimir Panajotov

***Abstract*—We present experimental and theoretical results of bistable polarization switching in a single transverse mode 1550 nm VCSEL subject to parallel optical injection. We focus our analysis on the bistability induced by power variation of the master laser found on the recently observed state of simultaneous injection locking of the parallel polarization mode and excitation of the orthogonal polarization mode, IL+PS. Experimental stability maps identifying, in the injected power-frequency detuning plane, where this state is observed, and corresponding bistable regions are reported for several bias currents. We find bistability between the IL+PS state and the single polarization mode injection locked solution. We also find bistability between the IL+PS and different periodic dynamics in the parallel polarization mode. The width of the hysteresis cycle increases when increasing the bias current or when increasing the wavelength of the optical injection beyond the solitary VCSEL wavelength. We theoretically confirm these types of bistability by numerically simulating the spin-flip model and by performing a linear stability analysis for the different stable states. Excellent agreement is found between experimental and theoretical results.**

***Index Terms*—Semiconductor lasers, Vertical-Cavity Surface-Emitting Lasers, Injection-locked lasers, Bistability.**

Manuscript received December, 2016. This work was funded by the Ministerio de Economía y Competitividad (MINECO/FEDER, UE), Spain under project TEC2015-65212-C3-1-P. The work of F. Denis-le Coarer and M. Sciamanna was supported by the Préfecture de Rgion Grand-Est through the projects FEDER (PHOTON, APOLLO) and FNADT (APOLLO, PIANO), and by AIRBUS-GDI Simulation, Metz Métropole, Conseil Départemental de Moselle, Conseil Régional Grand-Est, Préfecture de Région Grand-Est through the funding of the Chair in Photonics. The work of A. Quirce was supported by the Fonds Wetenschappelijk for the Post-Doctoral Fellowship. The work of H. Thienpont and K. Panajotov was supported by the Methusalem foundation.

F. Denis-le Coarer is with the Chair in Photonics, LMOPS laboratory, CentraleSupelec, Univ. of Paris-Saclay, and Univ. of Lorraine, 57070 Metz, France, and also with Instituto de Física de Cantabria (CSIC-Univ. Cantabria), Avda. Los Castros s/n, E39005, Santander, Spain. e-mail: florian.denis@supelec.fr

A. Quirce and H. Thienpont are with the Faculty of Engineering Sciences, Vrije Universiteit Brussel, 1050, Brussels, Belgium. e-mail: aquirce@b-phot.org; hthienpo@b-phot.org

P. Pérez, A. Valle, and L. Pesquera are with Instituto de Física de Cantabria (CSIC-Univ. Cantabria), Avda. Los Castros s/n, E39005, Santander, Spain. e-mail: pablopercu9@hotmail.com; valle@ifca.unican.es; pesquerl@ifca.unican.es

M. Sciamanna is with the Chair in Photonics, LMOPS laboratory, CentraleSupelec, Univ. of Paris-Saclay, and Univ. of Lorraine, 57070 Metz, France. e-mail: marc.sciamanna@centralesupelec.fr

K. Panajotov is with the Faculty of Engineering Sciences, Vrije Universiteit Brussel, 1050, Brussels, Belgium, and also with the Institute of Solid State Physics, Bulgarian Acadaemy of Sciences, 1784, Sofia, Bulgaria. e-mail: kpanajot@b-phot.org

I. Introduction

Vertical-cavity surface-emitting lasers (VCSELs) have attracted considerable interest in these last decades. This optical device, in comparison with edge emitting devices [1], [2], presents properties of particular interest as low fabrication costs, on-wafer testing capabilities, compactness leading to good potential for integration in two-dimensional arrays, low power consumption, high coupling efficiency to optical fibres, etc [1], [2]. VCSELs are intrinsically single-longitudinal mode devices. When lasing in the fundamental transverse mode, they can show two linear orthogonally polarized modes, and polarization switching (PS) between these two orthogonal modes can be observed with temperature or bias current changes [3]–[6]. Optical injection - a well known technique of improvement of semiconductor laser performance [7]–[9] - has been used on VCSEL to enhance their modulation bandwidth through the injection locking (IL) phenomenon [10], [11], but also to perform PS [12]–[17].

Bistability in laser diodes (see [18] and references therein) and more specifically in VCSELs subject to optical injection [19]–[27] has been the subject of a large amount of studies, mostly in view of possible exploitation for data transmission and all-optical signal processing. It has indeed been demonstrated that bistable VCSELs can be used as all optical memory [22], to perform all-optical shift register [23] and all-optical flip-flop operations [26], [27]. All-optical polarization switching bistability can be achieved by using orthogonal optical injection in VCSELs [19], [25] and is of great interest for photonic switching applications. Recently, experimental and theoretical demonstration of PS under parallel optical injection has been presented [28], [29]. In these previous works, a state was described in which both injection locking of the parallel polarization and excitation of the orthogonal polarization of the free-running VCSEL occur simultaneously [28], [29]. This state, termed as IL+PS, presents bistability properties [28], that are the subject of this work.

In this work we analyse experimentally and theoretically the bistability between the IL+PS solution and different injection locked and periodic solutions in which only the parallel polarization mode is excited. We present experimental and simulated stability maps of the IL+PS state in the injected power-frequency detuning plane obtained by sweeping the injected power, and corresponding hysteresis regions. We also perform the linear stability analysis developed by Friart

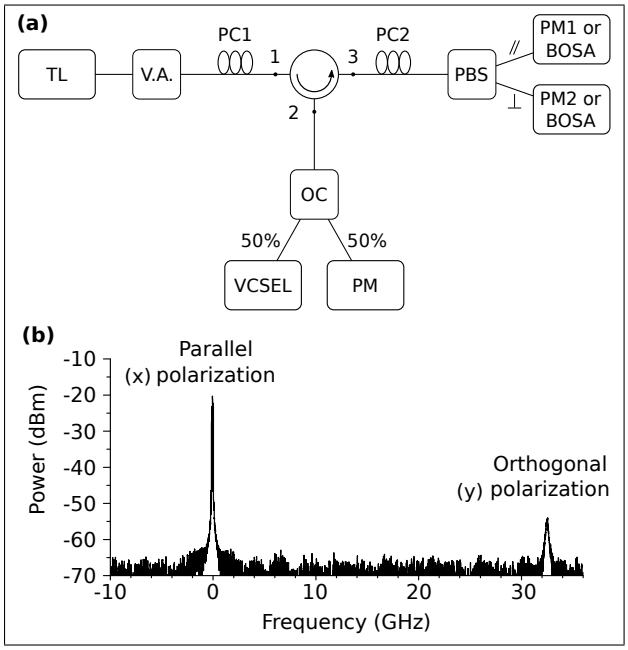

Fig. 1. **(a)** Experimental setup for parallel optical injection in the VCSEL. TL: tunable laser, PC1 and PC2: polarization controllers, VA: variable attenuator, OC: optical coupler, PBS: polarization beam splitter, PM: power meter, BOSA : high resolution optical spectrum analyser. **(b)** Experimental optical spectrum for the free-running VCSEL at 298 K and bias current I_{bias}=3.05 mA.

et al [30] for a mixed-mode steady state of an optically injected two-polarization modes edge emitting laser, that can be extended to the VCSEL case under the condition of adiabatically elimination of the spin dynamics [28], [29]. The linear stability analysis performed for the IL+PS state and the single polarization mode injection locked state (IL) gives very good agreement with experimental results.

The structure of this paper is organized as follows. We detail in section II the experimental setup used to perform parallel optical injection. In section III we present the experimental results. The theoretical model is described in section IV, and we present theoretical results in section V. And finally, section VI will be dedicated to the comparison between theoretical and experimental results.

II. Experimental Setup

Parallel optical injection is experimentally attained with the all-fiber setup shown in Fig. 1(a). The slave laser we use in the experiment (a 1550-nm wavelength VCSEL) is injected with the parallely polarized light from a master laser (tunable laser TL) via an optical three-port circulator and a polarization controller (PC1). We control the level of light injection using a digital variable attenuator (VA), and a power meter (PM) allows us to monitor the level of injected power, via a 50/50 optical coupler (OC). The third port of the optical circulator is connected to a second polarization controller (PC2) and a polarization beam splitter (PBS) allowing to select and separate orthogonal and parallel polarization beams, that are analysed by power meters (PM1 and PM2), or a high-resolution (10 MHz) optical spectrum analyser (BOSA).

The device used in the experiment as slave laser is a commercially available quantum-well long-wavelength (1550 nm) VCSEL (RayCan^{TM}), based on InAlGaAs active region. The temperature is held constant at 298 K for all the measurements. At this temperature, the threshold current of the VCSEL (I_{th}) is 1.66 mA. Fig. 1(b) shows the experimental optical spectrum of the free-running VCSEL for $I_{bias} = 3.05$ mA at 298 K. The two modes appearing in this spectrum are the two orthogonal polarizations of the fundamental single transverse mode. Higher order transverse modes are highly suppressed, more than 55 dB at this bias current. The laser emits in a linear polarization mode that we will call parallel polarization at a wavelength $\lambda_{/\!/} = 1540.91$ nm. The zero frequency has been chosen to correspond to this wavelength. The orthogonal linear polarization - the subsidiary mode - is shifted by 32.86 GHz toward the high frequencies, corresponding to 0.26 nm toward the short-wavelength side of the lasing mode to $\lambda_{\perp} = 1540.65$ nm with a side mode suppression ratio of 34 dB.

The free-running device shows several PSs for different values of the bias current : 2.25, 6.70, and 9.15 mA, type I, type II and type I PS, respectively. Type I PS is from the high-frequency to the low-frequency polarization and Type II PS is from the low-frequency to the high-frequency polarization [2]. We have considered multiple bias currents for our experiment remaining, however in a region in which there are no PSs for the free-running VCSEL. The optical injection from the TL is characterized by the value of the power P_i measured by the power meter PM (in Fig. 1(a)), and by the frequency detuning ν_i defined by the difference between the frequency of the injected light and the frequency of the lasing polarization mode of the free-running VCSEL.

III. Experimental Results

Fig. 2 presents two experimental optical spectra obtained for the same injection parameters ($\nu_i = -6.6$ GHz, $P_i = 422$ μW, and bias current $I_{bias} = 3.0$ mA) that correspond to two different states. Fig. 2(a) shows the IL+PS state presented in [28] in which injection locking of the parallel polarization and excitation of the orthogonal polarization occur simultaneously, and Fig. 2(b) shows the IL state, where only one peak that corresponds to the parallel polarization mode at the frequency of optical injection appears. These spectra were obtained for a fixed value of the frequency detuning, increasing and decreasing the value of injected power to obtain Fig. 2(a) and Fig. 2(b), respectively, thereby demonstrating hysteresis in the phenomenon. Bistability between a two-mode equilibrium state (TME) and the injection locked single mode solution has been observed in a two-color laser [31], [32]. There are some differences with respect to our case. IL+PS is observed in a single-mode laser, however, TME was observed in a two-mode laser. Also just a single linear polarization is excited in TME, however, in IL+PS the polarization behavior is more complex because two modes with orthogonal linear polarizations are excited.

We focus on the IL+PS state, and more specifically on the region of the injected power-frequency detuning plane where this state can be observed with its corresponding bistability regions. In order to characterize the region where IL+PS is

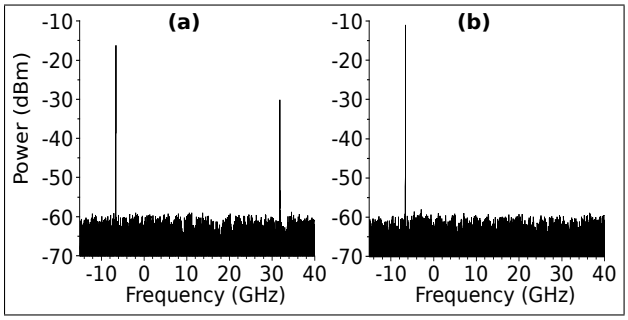

Fig. 2. Experimental optical spectra for injection parameters I_{bias}=3.0 mA, ν_i=−6.6 GHz, and P_i=422 μW when **(a)** increasing P_i (IL+PS state) and **(b)** decreasing P_i (IL state).

observed, we fix the value of the detuning ν_i, and increase the injection level from $P_i = 10$ nW to $P_i = 900$ μW, and then decrease the injected power back to its initial value. We repeat the process for several values of ν_i, recording for each value the range of P_i where the IL+PS state is observed, when increasing and decreasing the injection level. We perform this mapping of the parameters space for several bias currents, and results are shown in Fig. 3(a), Fig. 3(b), and Fig. 3(c) for $I_{bias} = 3.0$ mA, $I_{bias} = 4.0$ mA and $I_{bias} = 5.0$ mA respectively. In these maps, black (blue) lines identify an increase (decrease) of P_i, and thick (thin) lines identify the lower boundary as $P_{i,down}$ (higher boundary as $P_{i,up}$) of the region. For increasing P_i, IL+PS appears (disappears) at $P_{i,down}$ (at $P_{i,up}$). On the contrary, for decreasing P_i, IL+PS appears (disappears) at $P_{i,up}$ (at $P_{i,down}$). The state below $P_{i,down}$ usually corresponds to period-1 dynamics (P1) in the parallel polarization, except for $I_{bias} = 3.0$ mA, -4.2 GHz $< \nu_i <$ -3 GHz and $I_{bias} = 5.0$ mA, -5.2 GHz $< \nu_i < -4.4$ GHz, where a period doubling dynamics in this polarization (P2) is observed [33]. The state above $P_{i,up}$ is IL for negative values of ν_i, and various non-linear dynamics involving both polarization modes for positive values of ν_i. These various non-linear dynamics will be discussed in detail elsewhere [33].

We now focus on Fig. 3(a), mapping the IL+PS region for $I_{bias} = 3.0$ mA. Two regions where IL+PS can be observed appear both when increasing and decreasing the injection level P_i, one for negative values of ν_i ($\nu_i < -2$ GHz), and one for positive values of ν_i (0 GHz $< \nu_i <$ 2 GHz). For negative values of the frequency detuning $P_{i,down}$ and $P_{i,up}$ decrease monotonously with ν_i both when increasing or decreasing the injected power. There is an exception for $P_{i,down}$ when increasing the injection level, which presents a small non monotonous outgrowth region for -4.2 GHz $< \nu_i < -3$ GHz, the region where a period doubling dynamics in the parallel polarization is observed below $P_{i,down}$. In this region bistability between the IL+PS state and the parallel polarized period-2 solution is found, since $P_{i,down}$, for decreasing P_i, decreases in a monotonous way. Except for this region, bistability at the lower boundary of the IL+PS is not found. Bistability between IL+PS and IL states is also found for larger values of P_i. The width of this bistable region increases as $|\nu_i|$ increases. This width can be large: for instance, for $\nu_i = -7$ GHz it is close to 500 μW. We do not observe large bistability regions for

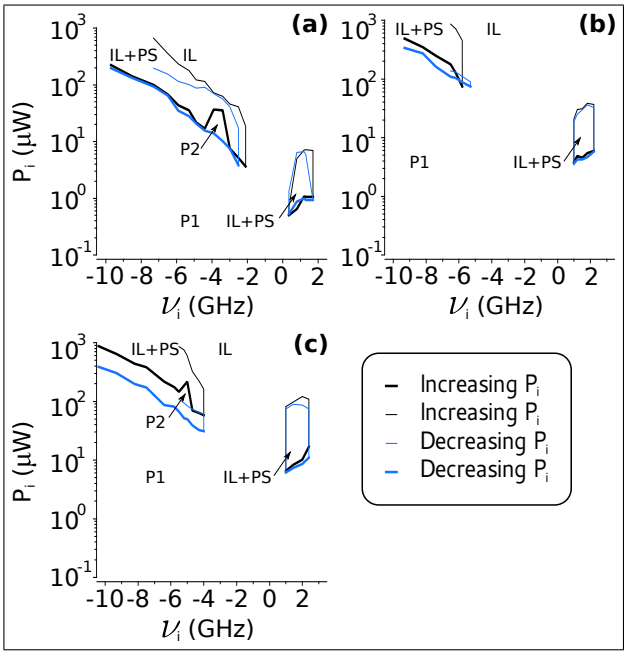

Fig. 3. Experimental values of the injected power for which IL+PS is observed for various bias currents **(a)** I_{bias}=3.0 mA, **(b)** I_{bias}=4.0 mA, and **(c)** I_{bias}=5.0 mA. Black (blue) identifies the increase (decrease) of the injection parameter P_i. $P_{i,down}$ and $P_{i,up}$ are identified with thick and thin lines, respectively.

positive values of ν_i.

We now focus on Fig. 3(b) and Fig. 3(c) that correspond to the map of the IL+PS state for $I_{bias} = 4.0$ mA and $I_{bias} = 5.0$ mA, respectively. For both bias currents we find again the two regions for positive and negative values of ν_i, but appearing for higher values of injected power. Indeed an increase of the bias current leads to a shift of the IL+PS region to higher values of injected powers. We can not obtain many points for $P_{i,up}$ for large negative values of ν_i because the maximum value of P_i in our experimental setup is 900 μW. Nevertheless, we can point out some general results. Bistability of the IL+PS state for positive values of the frequency detuning is still small, but becoming more appreciable for increasing bias currents (see Fig. 3(c)). For negative values of ν_i the width of the bistable region at the lower boundary increases with the bias current, which seems to be also the case for the higher boundary according to the few data we could record. Finally the negative value of the frequency detuning where the IL+PS state is last observed - respectively -2.1 GHz, -5.8 GHz and -4.0 GHz for $I_{bias} = 3.0,\ 4.0,\ 5.0$ mA - is not monotonous with regard to I_{bias}. We attribute this non monotonous behavior to the larger stable region of the period-2 solution found for $I_{bias} = 4.0$ mA: the system remains in this solution without jumping to the IL+PS state for $\nu_i > -5.8$ GHz.

IV. Theoretical Model

The theoretical study of the bistability corresponding to the IL+PS state is done with the commonly used spin-flip model (SFM) [34]. This rate equations model describes the polarization modes of a single mode VCSEL. The model equations are given in (1)-(4) in which we introduce an optical

injection term. In these equations, E_x and E_y are the two linearly polarized slowly varying components of the field in the x and y direction, corresponding to parallel and orthogonal polarizations, respectively. D and n are two carrier variables, corresponding to the total population inversion between conduction and valence band, and the difference between the population inversions for the spin-up and spin-down radiation channels [35], [36].

$$\begin{aligned}\frac{dE_x}{dt} &= -(\kappa+\gamma_a)E_x - i(\kappa\alpha+\gamma_p)E_x \\ &+ \kappa(1+i\alpha)(DE_x + inE_y) + \kappa E_{inj}e^{i2\pi\nu_{inj}t} \\ &+ \left(\sqrt{\frac{R_+}{2}}\xi_+(t) + \sqrt{\frac{R_-}{2}}\xi_-(t)\right) \qquad (1)\\ \frac{dE_y}{dt} &= -(\kappa-\gamma_a)E_y - i(\kappa\alpha-\gamma_p)E_y \\ &+ \kappa(1+i\alpha)(DE_y - inE_x) \\ &+ i\left(\sqrt{\frac{R_-}{2}}\xi_-(t) - \sqrt{\frac{R_+}{2}}\xi_+(t)\right) \qquad (2)\\ \frac{dD}{dt} &= -\gamma[D(1+|E_x|^2+|E_y|^2) - \mu \\ &+ in(E_yE_x^* - E_xE_y^*)] \qquad (3)\\ \frac{dn}{dt} &= -\gamma_s n - \gamma[n(|E_x|^2+|E_y|^2) \\ &+ iD(E_yE_x^* - E_xE_y^*)] \qquad (4)\end{aligned}$$

In this model, μ (see (5)) is the normalized bias current :

$$\mu = \frac{\tau_n}{\tau_e}\frac{\frac{I}{I_{th}} - 1}{1 - \frac{N_t}{N_{th}}} + 1 \qquad (5)$$

where I and I_{th} are respectively the bias current and the threshold currents, τ_n is the differential carrier lifetime at threshold ($\tau_n = 0.48$ ns), τ_e is the carrier lifetime at threshold ($\tau_e = 1.21$ ns), N_t and N_{th} are respectively the carrier number at transparency and threshold ($N_t = 9\times10^6$ and $N_{th} = 1.21\times10^7$) [37]. The other parameters of the SFM are given in table I. These parameters have been extracted for a similar free-running VCSEL in previous work [35], [37], and the linear dichroism γ_a of this VCSEL has been very recently extracted [29]. E_{inj} is the amplitude of the field of the injected light and ν_{inj} is the detuning between the injected light and the intermediate frequency between those of the x (parallel) and y (orthogonal) polarization, ν_x and ν_y, where $2\pi\nu_x = \alpha\gamma_a - \gamma_p$ and $2\pi\nu_y = \gamma_p - \alpha\gamma_a$. Thus the frequency detuning used to characterise the injected light in our experiment is $\nu_i = \nu_{inj} - \nu_x$.

Eqs. (1) and (2) take into account spontaneous emission noise rates, that are given by:

$$R\pm = \beta_{SF}\gamma\left[(D\pm n) + \frac{G_N N_t}{2\kappa}\right] \qquad (6)$$

where β_{SF} is the fraction of spontaneously emitted photons that are coupled into the laser mode ($\beta_{SF} = 6.5\times10^{-4}$) [35], G_N is the differential gain ($G_N = 2.152\times10^4$ s^{-1}), and

TABLE I
SPIN-FLIP MODEL PARAMETERS, ACCORDING TO [29], [37]

Parameter	Name	Value
κ	*Field decay rate*	33 ns^{-1}
γ_a	*Linear dichroism*	-0.21 ns^{-1}
α	*Linewidth enhancement factor*	2.8
γ_p	*Linear birefringence*	103.34 ns^{-1}
γ	*Decay rate of D*	2.08 ns^{-1}
γ_s	*Spin-flip relaxation rate*	2100 ns^{-1}

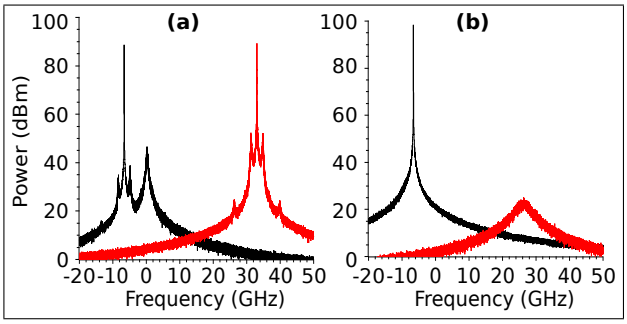

Fig. 4. Theoretical optical spectra for injection parameters I_{bias}=3.0 mA, ν_i=−6.6 GHz, and P_i=0.74 (a.u) when **(a)** increasing P_i (IL+PS state) and **(b)** decreasing P_i (IL state). Black (red) represents the parallel (orthogonal) polarization, respectively.

spontaneous emission induced fluctuations are included in our calculations with $\xi_+(t)$ and $\xi_-(t)$, that are complex Gaussian noise terms of zero mean and time correlation given by :

$$< \xi_i(t)\xi_j^*(t') >= \delta_{ij}\delta(t-t') \qquad (7)$$

Noise strengths of the circularly polarized e-field components are different in Eq. (6) because of the different carrier numbers in the two spin channels that participate in the optical transitions [3]. Spontaneous emission noise in the x and y linearly polarized components have the same strength but they have a correlation proportional to n. The value we use for γ_s, 2100 ± 500ns^{-1}, is obtained from measurements with a similar device [37]. This high value is within the very wide range of spin-flip rates reported in the literature, from a few tens to several thousand ns^{-1}. Although γ_s is large we have preferred to maintain the complete model in order to know the range of γ_s values for which we obtain similar results. Our simulations of Eqs. (1)-(6) indicate that results do not change if $\gamma_s > 300$ ns^{-1}. For these γ_s values n is small so it has not any relevant effect on the dynamics. Also the effect of having different noise strengths in Eq. (6) is negligible because n is small. We have preferred to maintain different noise strengths in order to see clearly the physical origin of both noises. So for our parameters the same results are obtained if n is not a dynamical variable (keeping n=0) and when uncorrelated noises with the same strength are used for both, x and y polarizations.

V. THEORETICAL RESULTS

We numerically integrate (1) to (4) with the parameter values of table I in order to obtain the theoretical spectra with similar injection parameters to those of Fig. 2. These injection parameters used to obtain Fig. 4 are $I = 3.0$ mA,

$\nu_i = -6.6$ GHz, and $\mathrm{P_i} = 0.74$ (a.u) $= 421$ μW. We use a conversion factor for the level of injection $\mathrm{P_i}$ of 1 (a.u) $\leftrightarrow$ 565.76 μW. The way of obtaining this factor is explained in the following section. The process to obtain the spectra of Fig. 4(a) and Fig. 4(b) is as follows. (1) to (4) have been integrated by using a continuous linear increase (decrease) of $\mathrm{P_i}$ from a small (large) initial value of $\mathrm{P_i}$ during 3 μs to the required value, $\mathrm{P_i} = 0.74$ (a.u.), at which the optical spectrum of Fig. 4(a) (Fig. 4(b)) is calculated. These spectrum are calculated using a 5 ps sampling time, an average over 20 temporal windows of 327.68 ns, and a 0.01 ps integration time step.

Fig. 4(a) shows that both the parallel and the orthogonal polarization modes are excited for these injection parameters when increasing the injected power. Parallel polarization is injection locked at frequency -6.6 GHz, and the orthogonal polarization mode of the free-running VCSEL is excited, thus implying that the system is in the IL+PS state. However, Fig. 4(b) shows that only the parallel polarization is locked to the injected light from the master laser when decreasing the injected power to reach the required value, so the system is in the IL state. This result confirms theoretically the results experimentally obtained and shown in Fig. 2. Some other tiny satellite peaks can be observed in Fig. 4(a). These peaks are excited due to the spontaneous emission noise and are experimentally below the noise level. We identify tiny peaks around each major peak of the parallel and orthogonal polarization, with a frequency separation 1.9 GHz, close to the theoretical relaxation oscillation frequency given by $(2\kappa\gamma(\mu - 1))^{1/2}/2\pi = 2.08$ GHz. Some other peaks are excited, as the parallel 0 frequency of the free-running VCSEL, and tiny peaks on each side of the main peak of each polarization with a frequency separation close to the detuning ν_i (respectively at -13.4, 26.2 and 40 GHz).

We now focus on the regions of the injected power-frequency detuning plane where the IL+PS state can be theoretically obtained by numerical integration of (1) to (4). In order to numerically characterize the IL+PS region in the parameters space, we set a process as close as possible to the experimental one. We fix a value of the detuning ν_i, and increase $\mathrm{P_i}$ from a low value to a large value, then decrease $\mathrm{P_i}$ again to its initial value. We increase the injected power from $\mathrm{P_{i,min}} = 10^{-5}$ (a.u) to $\mathrm{P_{i,max}} = 10$ (a.u) during 24.6 μs after a 80 ns transient (and a similar sweeping backwards). The injected power increases in exponential steps from $\mathrm{P_{i,min}}$ to $\mathrm{P_{i,max}}$ staying 375 ps on each step. Doing this sweep in $\mathrm{P_i}$, we record the value of $\mathrm{P_i}$ at which the power of the orthogonal linear polarization becomes larger (smaller) than 0.5 a.u., that is when we consider that the IL+PS state appears (disappears). After reaching $\mathrm{P_{i,max}}$ we decrease the injected power in a similar way recording again the values where IL+PS appears and disappears. This process is repeated for several values of the frequency detuning.

Results for several bias currents I =3.0, 4.0 and 5.0 mA are shown in Fig. 5(a), Fig. 5(b) and Fig. 5(c) respectively, with the same attributes as Fig. 3 with regards to the colors and the size of the lines. The three maps present similar behaviours to those in Fig. 3 with respect to several characteristics. As in the

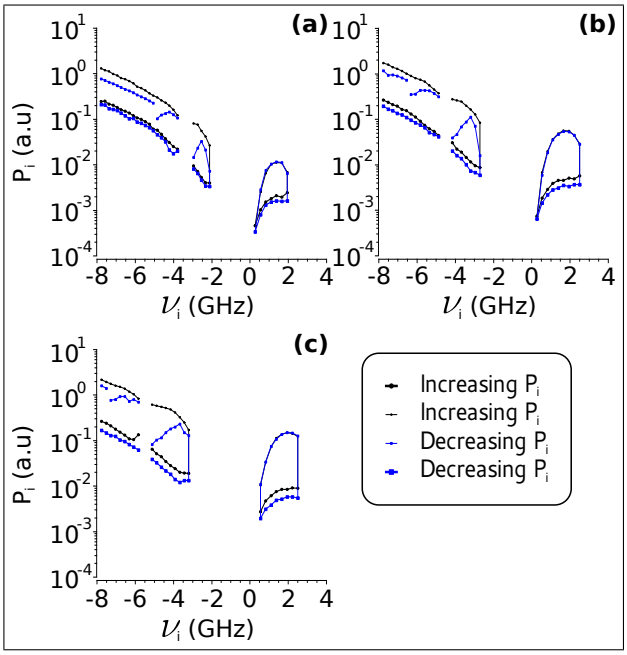

Fig. 5. Numerically simulated values of the injected power for which IL+PS is observed for various bias currents **(a)** I=3.0 mA, **(b)** I=4.0 mA, and **(c)** I=5.0 mA. Black (blue) identifies the increase (decrease) of the injection parameter $\mathrm{P_i}$. $\mathrm{P_{i,down}}$ and $\mathrm{P_{i,up}}$ are identified with thick and thin lines, respectively.

experimental maps, two separated regions can be observed for negative and positive values of ν_i, both when increasing and decreasing the injection level, with almost the same extrema values of ν_i, except for the case $I = 4.0$ mA. Similarly to the experimental maps, the regions are shifted upwards with an increase of the bias current, and the width of the region also increase with I. The shape of the regions is relatively similar for the different bias currents, both when increasing or decreasing the injected power. For negative values of ν_i, $\mathrm{P_{i,down}}$ is monotonously decreasing for all the bias currents, both when increasing and decreasing $\mathrm{P_i}$, and the size of the bistable region of $\mathrm{P_{i,down}}$ increases with I which confirm our experimental results, given in Fig. 3. Some similarities and differences appear at the boundary between IL+PS and IL. On one hand $\mathrm{P_{i,up}}$ when increasing the level of injection (thin black lines) monotonously decrease with ν_i for all bias currents, similarly to the experiment. However, $\mathrm{P_{i,up}}$ when decreasing $\mathrm{P_i}$ is non-monotonous in this region. Bistability between IL+PS and IL is obtained, but the shape of $\mathrm{P_{i,up}}$ when decreasing $\mathrm{P_i}$ and thus the shape of the bistable region is quite different to the experimental results. Fig. 5 also shows that there are regions around ν_i=-3.2, -4.4 and -5.2 GHz for I =3.0, 4.0 and 5.0 mA, respectively, at which no transitions to IL+PS are observed. In these regions, similarly to the experiment, period doubling dynamics in the parallel polarization are observed before reaching the IL state. However no transitions to IL+PS appear in simulations. In the experiments there is bistability between the period-2 and IL+PS solutions. In this way the initial conditions in the theory can be different to those of the experiment and transition to IL+PS is not observed. In fact, the non monotonous outgrowth region of Fig. 3(a) around

-3.2 GHz shows that also in the experiments the transition to IL+PS is almost not reached.

We now perform a linear stability analysis of both, the IL+PS and IL states in order to study the bistable behavior. This stability analysis has been recently done for a two-polarization mode edge-emitting semiconductor laser modelled by the following dimensionless rate equations subject to TE-polarized optical injection [30].

$$\frac{dE_1}{ds} = (1+i\alpha)NE_1 + \overline{\gamma}e^{i\Delta s} \tag{8}$$

$$\frac{dE_2}{ds} = (1+i\alpha)\overline{\kappa}(N-\beta)E_2 \tag{9}$$

$$T\frac{dN}{ds} = P - N - (1+2N)\left(|E_1|^2 + |E_2|^2\right) \tag{10}$$

where E_1, E_2, and N are the amplitude of the TE (corresponding to the x polarization) electric field, the amplitude of the TM (y polarization) electric field, and carrier density, respectively. s is a time parameter, T is the ratio of carrier to cavity lifetimes, P is the pump parameter, $\overline{\gamma}$ is the injection strength, Δ is the frequency detuning between the injected signal and the solitary laser, $\overline{\kappa}$ is the ratio of the gain coefficients of the TM and TE modes, and β measures the losses of the TM mode compared to the TE mode. The analysis done in [30] can be extended to the model detailed in Eqs. (1) to (4) because the spin-flip relaxation rate is very large [35] and therefore n is very small [28]. If we make the approximation $n = 0$ in Eqs. (1) to (4) and the following change of variables: $E_x = \sqrt{2}E_1\exp(-i(\gamma_p - \alpha\gamma_a)t)$, $E_y = \sqrt{2}E_2\exp(i(\gamma_p - \alpha\gamma_a)t)$, $D = (2N+1)(1+\gamma_a/\kappa)$, and $t = s/(2\kappa(1+\gamma_a/\kappa))$ we obtain the model of Eqs. (8)-(10). The parameters relation with respect to the model of Eqs. (1)-(4) is given in [29]. The approximation is reasonable because n oscillates around the zero value with a very small amplitude, of the order of 10^{-4}, when Eqs. (1)-(4) are used to describe IL+PS. The stability of the IL+PS state - corresponding to the mixed mode TE+TM in [30] - is given by the Routh-Hurwitz condition (Eq. (18) to Eq. (20) in [30]). This condition in our model gives the Hopf bifurcation from the two-modes steady-state (H_2 lines in [30]).

Fig. 6(a) presents a comparison between the H_2 bifurcation curves (red lines) and the numerically simulated maps (blue symbols) in the injected power-frequency detuning plane. More specifically, the simulated boundaries are those obtained when increasing the level of injection for the higher boundary, and the one obtained when decreasing P_i for the lower boundary, corresponding respectively for each ν_i to the higher and lower values of injected power for which the IL+PS state is obtained. We can see in this figure that the agreement is very good with the exception of the ν_i region around -3.2 GHz, as already explained.

In Fig. 6(b) are presented both the Hopf bifurcation of the IL+PS state (H_2 in red) and the results obtained with the linear stability analysis of the TE steady state (IL in our case), according to the Routh-Hurwitz condition given in Eq. (13) to Eq. (15) of [30], and extended to our model (SN_1 for the saddle-node bifurcation and H_1 for the Hopf bifurcation in black). This figure shows that for $\nu_i < -3.5$ GHz, there is a region where both IL and IL+PS can be stable, inducing bistability between these two states in this region. This region is qualitatively very similar to the experimental region of bistability between IL and IL+PS. Comparison maps will be given in the following section.

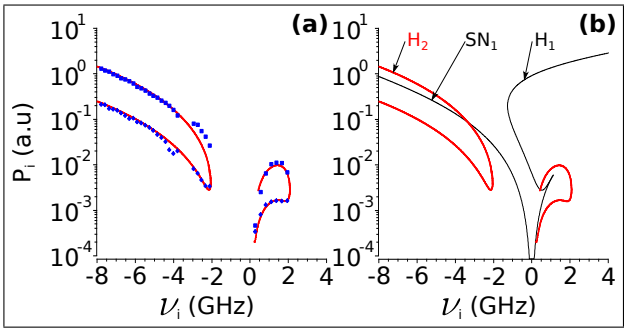

Fig. 6. **(a)** Comparison between IL+PS region obtained by numerical integration of (1) to (4) (in blue) and IL+PS region obtained by the linear stability analysis of the IL+PS steady state (in red) for bias current $I = 3.0$ mA. **(b)** Theoretical values of the injected power for which IL+PS state can be obtained as a function of ν_i for $I = 3.0$ mA in red lines. Black lines represent the theoretical boundaries of the region for which injection locked state is stable according to [30].

VI. Analysis and Comparison Theory-Experiment

Fig. 6(b) shows that optical bistability between IL+PS and IL solutions appears because H_2 and SN_1 bifurcation lines do not coincide. Fig. 7(a) and Fig. 7(b) present a comparison between Fig. 6(b) and the experimental mapping of both the IL+PS region and the IL region, respectively when increasing and decreasing the level of injected power, in blue symbols in the two figures. A single conversion factor 1 (a.u) $\leftrightarrow$ 565.76 μW has been applied to the experimental values in order to compare theoretical and experimental maps. Transitions between different dynamical regimes are observed and labelled as follows. IL+PS/IL transition (filled squares) is mainly observed for large and negative values of ν_i and in a small region close to ν_i=0.5 GHz. Very good agreement is found with our theoretical results with the exception of Fig. 7(b) in which experimental values are below the SN_1 bifurcation line: although qualitatively the bistability between IL+PS and IL states is well described by the model, we obtain wider experimental hysteresis cycles. The transition between period-1 dynamics in the parallel polarization and IL+PS (filled rhombuses), that we call P1/IL+PS, appears both in Fig. 7(a) and in Fig. 7(b) and for positive and negative values of ν_i. Good agreement between experiment and the theoretical values of the H_2 boundary is found.

More transitions involving the IL+PS state are shown in Fig. 7. A transition appears between period-2 dynamics in the parallel polarization and IL+PS (P2/IL+PS, open circles), that was already described in section 3. This transition closely follows the lower H_2 boundary except for -4.2 GHz $< \nu_i < -3$ GHz in Fig. 7(a) due to bistability between P2 and IL+PS. We also find transitions between period-1 dynamics in both polarizations and IL+PS (P1 both/IL+PS, filled triangles) and between period-2 dynamics in both polarizations and

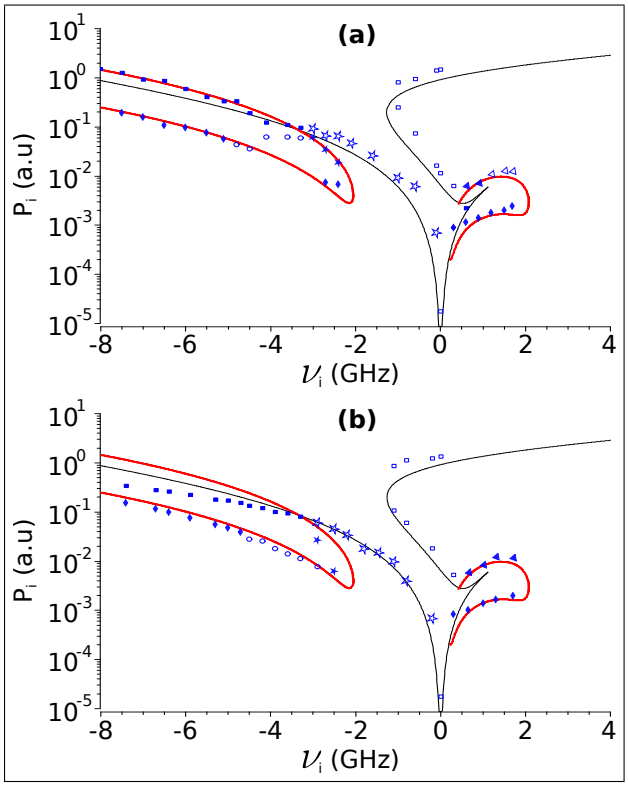

Fig. 7. Comparison between theoretical boundaries of the IL+PS and IL states in the (P_i,ν_i) plane for $I_{bias} = 3.0$ mA on one hand, and experimental values of the same boundaries (symbols) when **(a)** increasing P_i and **(b)** decreasing P_i. Experimental transitions are (■) IL+PS/IL, (⧫) P1/IL+PS, (○) P2/IL+PS, (▲) P1 both/IL+PS, (△) P2 both/IL+PS, (★) CH/IL+PS, (□) P1/IL, and (☆) CH/IL.

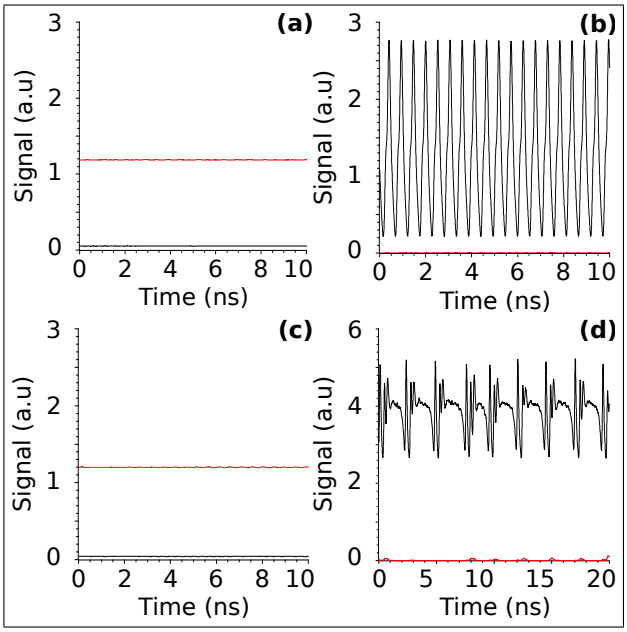

Fig. 8. Numerical time series of the intensity in both polarizations for a 3mA bias current and (a) ν_i=-3.8 GHz, P_i=0.03 (a.u.), (b) ν_i=-3.8 GHz, P_i=0.02 (a.u.), (c) ν_i=-2.2 GHz, P_i=0.009 (a.u.), and (d) ν_i=-2.2 GHz, P_i=0.022 (a.u.). Black (red) represents the parallel (orthogonal) polarization, respectively.

IL+PS (P2 both/IL+PS, open triangles). These transitions coincide with the upper H_2 boundary at positive ν_i. Also we find a transition between chaotic dynamics in the parallel polarization and IL+PS (CH/IL+PS, filled stars) that closely follows the H_2 boundary in Fig. 7(a). We also find two more transitions involving the IL state. The first is between period-1 dynamics in the parallel polarization and IL (P1/IL, open squares), and the second is between chaotic dynamics in the parallel polarization and IL (CH/IL, open stars). Good agreement between experiment and theory is found because P1/IL (CH/IL) follows the H_1 (SN_1) line.

Figure 8 shows results, obtained from simulation of the SFM model, of the intensity dynamics in both polarizations in order to illustrate different dynamical states included in Fig. 7. Fig. 8 shows how decreasing the injected power can change the IL+PS state (Fig. 8(a)) to a period-1 solution in the parallel polarization (Fig. 8(b)). Fig. 8 also illustrates the change from the IL+PS state (Fig. 8(c)) to a chaotic dynamics in the parallel polarization (Fig. 8(d)) obtained when the injected power is increased.

There are some considerations to be taken into account when comparing theoretical and experimental results. As already explained bistability can induce differences in the observed behaviours due to the different initial conditions in theory and in experiments. Also the criterium to specify if IL+PS is observed is different. In simulations the time at which the power of the orthogonal linear polarization crosses a threshold defines when IL+PS appears. However in experiments the optical spectrum, that is an averaged quantity over long time traces, is used. Moreover, in obtaining the analytical results some assumptions are taken into account, like the absence of noise, $n = 0$, and an instantaneous change of injected power, that are not satisfied in the experiment. However, in general we find good agreement, even sometimes quantitative, between theoretical and experimental results in our system.

We have also analysed the reproducibility of our results by making more measurements with another similar VCSEL with 27.48 GHz birefringence and 1.48 mA threshold current. Results shown in Fig.2, Fig. 3, and Fig. 7 are qualitatively similar. Quantitative comparison is also reasonable because shifts in boundaries are such that large hysteresis widths are also found. For instance, the results that are obtained in Fig. 3(c) for -5.3 GHz frequency detuning are similar to those obtained with the new device at -6.4 GHz detuning for the same value of the normalized bias current of Fig. 3(c), that is three times threshold.

The model parameters that we use have been extracted for a commercial VCSEL (RayCan) similar to the device used in this work. There are some other references that have found values of κ and γ_s similar to the values we use. For instance κ=29 ns^{-1} for a similar RayCan VCSEL [38], and κ=25 ns^{-1} for another 1550-nm VCSEL [39]. These values are similar to the one we use,κ=33 ns^{-1} Also $\gamma_s = 620ns^{-1}$ [38] and $\gamma_s = 1000ns^{-1}$ [40] have been measured, both for RayCan VCSELs. These values are of the same order than our value. We have also made further simulations of the SFM model using more typical values, κ=300 ns^{-1} and $\gamma_s = 50ns^{-1}$ [34]. We observe no transition to IL+PS state when increasing

the injected power for a situation (ν_i=-6.5 GHz, I= 3mA) in which we observe a transition to IL+PS state in experiments and in simulations with the parameters of Table I.

VII. Summary and Conclusions

We have reported in this paper an experimental and theoretical analysis of the bistability properties of the IL+PS state, that is a state in which simultaneous injection locking of the parallel polarization mode and excitation of the orthogonal polarization mode appear when a VCSEL is subject to parallel optical injection. This state is unusual because optical injection in the polarization with smaller optical losses causes emission in the polarization with larger losses. For the usual injection locked single-mode laser diode the solution with population inversion larger than 1 (y-linear polarization with larger losses) is unstable. However, when considering a two polarization modes VCSEL below the IL+PS region of Fig. 7(a), period-1 dynamics is observed in such a way that D oscillates with an amplitude that increases as the injected power increases. In this way, as the system gets closer to the IL+PS region, D oscillates reaching values well above 1. The two-mode solution (IL+PS state) with $D_y = 1 - \gamma_a/\kappa$ may become stable for certain injection strengths and frequency detunings while the period-1 solution destabilizes.

We have analyzed the bistability induced by power variation of the master laser for a fixed frequency detuning. Stability maps in the injected power-frequency detuning plane in which IL+PS is observed have been measured and calculated. We have found several types of bistabilities. We have focused our attention in two of them: i) bistability between the IL+PS state and the single polarization mode injection locked solution (IL), and ii) bistability between the IL+PS and periodic dynamics in the parallel polarization mode. For i) case we have made a complete experimental, numerical and a linear stability analysis of both IL+PS and IL solutions. For ii) case we have just compared numerical simulation with experimental results. In both cases the width of the hysteresis cycle increases when increasing the bias current or when increasing the wavelength of the optical injection beyond the solitary VCSEL wavelength. In general the agreement between experimental and theoretical results is very good. Better overall agreement is found between our experimental results and those derived from the linear stability analysis.

The bistability between IL and IL+PS has the benefit to be easily experimentally measured. We have found large hysteresis widths, more than 500 μW, with very good reproducibility, which makes this polarization switching bistability induced by optical injection of interest with respect to all-optical data processing applications.

Acknowledgment

A. Quirce acknowledges Fonds Wettenschapplijk fellowship and H. Thienpont and K. Panajotov are grateful to the Methusalem foundation for financial support.

References

[1] F. Koyama, "Recent advances of VCSEL photonics," *Journal of Lightwave Technology*, vol. 24, no. 12, pp. 4502–4513, 2006.

[2] R. Michalzik, *VCSELs: fundamentals, technology and applications of vertical-cavity surface-emitting lasers*. Springer, 2012, vol. 166.

[3] M. San Miguel, Q. Feng, and J. V. Moloney, "Light-polarization dynamics in surface-emitting semiconductor lasers," *Physical Review A*, vol. 52, no. 2, p. 1728, 1995.

[4] A. Valle, L. Pesquera, and K. Shore, "Polarization behavior of birefringent multitransverse mode vertical-cavity surface-emitting lasers," *IEEE Photonics Technology Letters*, vol. 9, no. 5, pp. 557–559, 1997.

[5] K. Panajotov, B. Ryvkin, J. Danckaert, M. Peeters, H. Thienpont, and I. Veretennicoff, "Polarization switching in VCSEL's due to thermal lensing," *IEEE Photonics Technology Letters*, vol. 10, no. 1, pp. 6–8, 1998.

[6] B. Ryvkin, K. Panajotov, A. Georgievski, J. Danckaert, M. Peeters, G. Verschaffelt, H. Thienpont, and I. Veretennicoff, "Effect of photon-energy-dependent loss and gain mechanisms on polarization switching in vertical-cavity surface-emitting lasers," *J. Opt. Soc. Amer. B*, vol. 16, no. 11, pp. 2106–2113, 1999.

[7] R. Lang, "Injection locking properties of a semiconductor laser," *IEEE Journal of Quantum Electronics*, vol. 18, no. 6, pp. 976–983, 1982.

[8] G. Van Tartwijk and D. Lenstra, "Semiconductor lasers with optical injection and feedback," *Quantum and Semiclassical Optics: Journal of the European Optical Society Part B*, vol. 7, no. 2, p. 87, 1995.

[9] S. Wieczorek, B. Krauskopf, T. Simpson, and D. Lenstra, "The dynamical complexity of optically injected semiconductor lasers," *Physics Reports*, vol. 416, no. 1, pp. 1–128, 2005.

[10] C.-H. Chang, L. Chrostowski, and C. J. Chang-Hasnain, "Injection locking of VCSELs," *IEEE Journal of Selected Topics in Quantum Electronics*, vol. 9, no. 5, pp. 1386–1393, 2003.

[11] L. Chrostowski, B. Faraji, W. Hofmann, M.-C. Amann, S. Wieczorek, and W. W. Chow, "40 GHz bandwidth and 64 GHz resonance frequency in injection-locked 1.55 μm VCSELs," *IEEE Journal of Selected Topics in Quantum Electronics*, vol. 13, no. 5, pp. 1200–1208, 2007.

[12] Y. Hong, K. Shore, A. Larsson, M. Ghisoni, and J. Halonen, "Polarisation switching in a vertical cavity surface emitting semiconductor laser by frequency detuning," *IEEE Proceedings-Optoelectronics*, vol. 148, no. 1, pp. 31–34, 2001.

[13] J. B. Altés, I. Gatare, K. Panajotov, H. Thienpont, and M. Sciamanna, "Mapping of the dynamics induced by orthogonal optical injection in vertical-cavity surface-emitting lasers," *IEEE Journal of Quantum Electronics*, vol. 42, no. 2, pp. 198–207, 2006.

[14] K. H. Jeong, K. H. Kim, S. H. Lee, M. H. Lee, B.-S. Yoo, and K. A. Shore, "Optical injection-induced polarization switching dynamics in 1.5-μm wavelength single-mode vertical-cavity surface-emitting lasers," *IEEE Photonics Technology Letters*, vol. 20, no. 10, pp. 779–781, 2008.

[15] A. Hurtado, I. D. Henning, and M. J. Adams, "Two-wavelength switching with a 1550 nm VCSEL under single orthogonal optical injection," *IEEE Journal of Selected Topics in Quantum Electronics*, vol. 14, no. 3, pp. 911–917, 2008.

[16] A. Hurtado, A. Quirce, A. Valle, L. Pesquera, and M. J. Adams, "Nonlinear dynamics induced by parallel and orthogonal optical injection in 1550 nm vertical-cavity surface-emitting lasers (VCSELs)," *Optics Express*, vol. 18, no. 9, pp. 9423–9428, 2010.

[17] M. Nizette, M. Sciamanna, I. Gatare, H. Thienpont, and K. Panajotov, "Dynamics of vertical-cavity surface-emitting lasers with optical injection: a two-mode model approach," *J. Opt. Soc. Amer. B*, vol. 26, no. 8, pp. 1603–1613, 2009.

[18] H. Kawaguchi, "Bistable laser diodes and their applications: state of the art," *IEEE Journal of Selected Topics in Quantum Electronics*, vol. 3, no. 5, pp. 1254–1270, 1997.

[19] Z. G. Pan, S. Jiang, M. Dagenais, R. A. Morgan, K. Kojima, M. T. Asom, R. E. Leibenguth, G. D. Guth, and M. W. Focht, "Optical injection induced polarization bistability in vertical-cavity surface-emitting lasers," *Applied Physics Letters*, vol. 63, no. 22, pp. 2999–3001, 1993.

[20] T. Mori, Y. Yamayoshi, and H. Kawaguchi, "Low-switching-energy and high-repetition-frequency all-optical flip-flop operations of a polarization bistable vertical-cavity surface-emitting laser," *Applied Physics Letters*, vol. 88, no. 10, p. 101102, 2006.

[21] A. Valle, M. Gomez-Molina, and L. Pesquera, "Polarization bistability in 1550 nm wavelength single-mode vertical-cavity surface-emitting lasers subject to orthogonal optical injection," *IEEE Journal of Selected Topics in Quantum Electronics*, vol. 14, no. 3, pp. 895–902, 2008.

[22] J. Sakaguchi, T. Katayama, and H. Kawaguchi, "All-optical memory operation of 980-nm polarization bistable VCSEL for 20-Gb/s PRBS RZ and 40-Gb/s PRBS NRZ data signals," *Optics Express*, vol. 18, no. 12, pp. 12 362–12 370, 2010.
[23] T. Katayama, D. Hayashi, and H. Kawaguchi, "All-optical shift register using polarization bistable VCSEL array," *IEEE Photonics Technology Letters*, vol. 28, no. 19, pp. 2062–2065, 2016.
[24] A. Hurtado, A. Quirce, A. Valle, L. Pesquera, and M. J. Adams, "Power and wavelength polarization bistability with very wide hysteresis cycles in a 1550nm-VCSEL subject to orthogonal optical injection," *Optics Express*, vol. 17, no. 26, pp. 23 637–23 642, 2009.
[25] B. Ryvkin, K. Panajotov, E. Avrutin, I. Veretennicoff, and H. Thienpont, "Optical-injection-induced polarization switching in polarization-bistable vertical-cavity surface-emitting lasers," *Journal of Applied Physics*, vol. 96, no. 11, pp. 6002–6007, 2004.
[26] S. H. Lee, H. W. Jung, K. H. Kim, M. H. Lee, B.-S. Yoo, J. Roh, and K. A. Shore, "1-GHz all-optical flip-flop operation of conventional cylindrical-shaped single-mode VCSELs under low-power optical injection," *IEEE Photonics Technology Letters*, vol. 22, no. 23, pp. 1759–1761, 2010.
[27] T. Katayama, K. Nakao, D. Hayashi, and H. Kawaguchi, "Flip-flops using polarization bistable VCSEL with AND-gate functionality by two wavelength inputs," *IEICE Electronics Express*, vol. 13, no. 5, pp. 1–6, 2016.
[28] A. Quirce, P. Pérez, A. Popp, Á. Valle, L. Pesquera, Y. Hong, H. Thienpont, and K. Panajotov, "Polarization switching and injection locking in vertical-cavity surface-emitting lasers subject to parallel optical injection," *Optics Letters*, vol. 41, no. 11, pp. 2664–2667, 2016.
[29] A. Quirce, A. Popp, F. Denis-le Coarer, P. Pérez, Á. Valle, L. Pesquera, Y. Hong, H. Thienpont, K. Panajotov, and M. Sciamanna, "Analysis of the polarization of single-mode vertical-cavity surface-emitting lasers subject to parallel optical injection," *J. Opt. Soc. Amer. B*, vol. 34, no. 2, pp. 447–455, 2017.
[30] G. Friart, A. Gavrielides, and T. Erneux, "Analytical stability boundaries of an injected two-polarization semiconductor laser," *Physical Review E*, vol. 91, no. 4, p. 042918, 2015.
[31] S. Osborne, K. Buckley, A. Amann, and S. O'Brien, "All-optical memory based on the injection locking bistability of a two-color laser diode," *Optics Express*, vol. 18, no. 8, pp. 6293–6300, 2009.
[32] D. O'Shea, S. Osborne, N. Blackbeard, G. Goulding, B. Kelleher, and A. Amann, "Experimental classification of dynamical regimes in optically injected lasers," *Optics Express*, vol. 22, no. 18, pp. 21 701–21 710, 2014.
[33] F. Denis-le Coarer, A. Quirce, Á. Valle, L. Pesquera, M. Sciamanna, H. Thienpont, and K. Panajotov, "Polarization dynamics induced by parallel optical injection in a single-mode VCSEL," *Optics Letters*, Submitted.
[34] J. Martin-Regalado, F. Prati, M. San Miguel, and N. Abraham, "Polarization properties of vertical-cavity surface-emitting lasers," *IEEE Journal of Quantum Electronics*, vol. 33, no. 5, pp. 765–783, 1997.
[35] P. Pérez, A. Valle, and L. Pesquera, "Polarization-resolved characterization of long-wavelength vertical-cavity surface-emitting laser parameters," *J. Opt. Soc. Amer. B*, vol. 31, no. 11, pp. 2574–2580, 2014.
[36] P. Pérez, A. Quirce, A. Valle, A. Consoli, I. Noriega, L. Pesquera, and I. Esquivias, "Photonic generation of microwave signals using a single-mode VCSEL subject to dual-beam orthogonal optical injection," *IEEE Photonics Journal*, vol. 7, no. 1, pp. 5 500 614–14, 2015.
[37] P. Pérez, A. Valle, I. Noriega, and L. Pesquera, "Measurement of the intrinsic parameters of single-mode VCSELs," *Journal of Lightwave Technology*, vol. 32, no. 8, pp. 1601–1607, 2014.
[38] Y. Ji-Yun, W. Zheng-Mao, L. Qing, C. Jian-Jun, Z. Zhu-Qiang, and X. Guang-Qiong, "Experimental determination of key parameters in the spin-flip model of 1550 nm vertical cavity surface-emitting laser," *Acta Physica Sinica*, vol. 65, p. 124203, 2016.
[39] V. M. Deshmukh, S. H. Lee, D. W. Kim, K. H. Kim, and M. H. Lee, "Experimental and numerical analysis on temporal dynamics of polarization switching in an injection-locked 1.55-μm wavelength vcsel," *Opt. Express*, vol. 19, no. 18, pp. 16 934–16 949, Aug 2011.
[40] R. Al-Seyab, K. Schires, A. Hurtado, I. D. Henning, and M. J. Adams, "Dynamics of vcsels subject to optical injection of arbitrary polarization," *IEEE Journal of Selected Topics in Quantum Electronics*, vol. 19, no. 4, pp. 1 700 512–1 700 512, July 2013.

PLACE PHOTO HERE

Florian Denis le Coarer was born in France in 1992. He received the Engineering degree from CentraleSupelec (France), and a Masterś degree from the University of Lorraine (France) in 2016, both with a major in photonics. He is currently pursuing the Ph.D. degree with CentraleSupelec (France). His current research interests include dynamics of vertical-cavity surface-emitting lasers and non-linear dynamics of other photonic systems.

PLACE PHOTO HERE

Ana Quirce received the Licenciada en Física (M.Sc.) degree and the Ph.D. degree in sciences, technologies, and computing from the University of Cantabria, Santander, Spain, in 2008 and 2012, respectively, where she was studying the dynamics of the polarization and transverse modes of vertical cavity surface-emitting lasers (VCSELs) subject to optical injection. She is currently a Post-Doctoral Fellow from the Research Foundation-Flanders (FWO) with the Vrije Universiteit Brussel, Brussels, Belgium. Her current research interests are in the areas of dynamics of VCSELs, optical injection effects in semiconductor lasers, optical feedback, optical frequency combs, and photonic integrated circuits.

PLACE PHOTO HERE

Pablo Pérez received the Ms degree in Physics from the Universidad de Cantabria, Spain, in 2010. He recieved the Ph.D. degree in physics from the Universidad de Cantabria, Spain in 2015.

PLACE PHOTO HERE

Angel Valle received the M. Sc. and Ph.D. degree in Physics from the Universidad de Cantabria, Spain, in 1988 and 1993, respectively. During 1994 and 1995, he was a postdoctoral fellow at the School of Electronic and Electrical Engineering at the University of Bath, England. In 1996 he joined the Instituto de Física de Cantabria (CSIC-UC). Since 1998 he has been lecturer at the Departamento de Física Moderna at the University of Cantabria, Spain. His research interests are in the areas of vertical-cavity surface-emitting lasers, noise and nonlinear dynamics of semiconductor lasers.

PLACE PHOTO HERE

Luis Pesquera received the M.Sc. degree in physics in 1974 from the Universidad de Valladolid, Spain. He was a postgraduate fellow at the Universit de Paris VI during 1977-1980. He received the Ph. D. degree in physics in 1980 from the Universidad de Cantabria, Santander, Spain. In 1980 he joined the Departamento de Fsica Moderna of the Universidad de Cantabria. Since 1991 he has been Professor of Physics at the Universidad de Cantabria. In 1995 he joined the Instituto de Física de Cantabria (CSIC–UC). His research work started in the field of stochastic processes applied to Physics and he has made contributions to the foundations of quantum physics, fluctuations in nuclear reactors, disordered systems and laser physics. His current research interests include semiconductor laser dynamics, vertical-cavity surface-emitting lasers and bio-inspired information processing.

PLACE PHOTO HERE

Marc Sciamanna graduated in electrical engineering in 2000 and received the Ph.D. degree in applied sciences in 2004 from Facult Polytechnique de Mons, Arrondissement of Mons, Belgium. In 2009, he received the Habilitation Diriger les Recherches (HDR) from University Paul Verlaine, Metz, France (now called University of Lorraine) in 2012. In 2004, he became an Assistant Professor and since 2009, Full Professor at Suplec, France. He is the Head of the Optics and Electronics (OPTEL) Research Group, Suplec, and since 2012, he has been the Adjunct Director of the LMOPS Laboratory (Laboratoire Matriaux Optiques, Photonique et Systmes, EA-4423). He has authored about 150 publications, including 60 publications in peer-reviewed journals. His current research interests include theory and experiment on nonlinear dynamics of semiconductor lasers with optical injection or optical feedback, optical chaos and chaos synchronization in coupled oscillators, control of optical pattern formation in photorefractive nonlinear cavities, phase conjugate optical feedback effects, polarization properties of VCSELs. He was a recipient of the IEEE-LEOS (now IEEE Photonics Society) in 2002 with a Graduate Student Fellowship Award, the International Society for Optical Engineering (SPIE) in 2003 with the F-MADE Scholarship Award, and the Optical Society of America (OSA) in 2002 with a OSA Newfocus Student Travel Grant. In 2007, he received the TR35 Young Innovator Award from MIT Technology Review (U.S.A.) for his work on controlling chaos in telecom lasers. He is also a Chairman and Committee Member of several international conferences, including SPIE Photonics Europe (2008, 2010, 012), the EOS Annual Meeting (2010, 2012), the IEEE/LEOS Winter Topicals (2009), the IEEE International Semiconductor Laser Conference (2012), PHASE/IPSSO international workshops (2005, 2007) and A Future in Light international conference (2009). He is also an Associate Editor for the international journal Optical and Quantum Electronics, edited by Springer.

PLACE PHOTO HERE

Hugo Thienpont (M99) was born in Ninove, Belgium, in 1961. He received the Academic degree in electrotechnical engineering and the Ph.D. degree in applied sciences from Vrije Universiteit Brussel (VUB), Brussels, Belgium, in 1984 and 1990, respectively. He became a Professor at the Faculty of Applied Sciences, with teaching responsibilities in photonics in 1994. In 2000, he became the Research Director of the Department of Applied Physics and Photonics at VUB, and in 2004, he was elected as the Chair of the Department of Applied Physics and Photonics. He is currently the Coordinator of several basic research and networking projects, such as the European Access to Micro-Optics Expertise, Services and Technologies network. In addition to academic-oriented research projects, he manages microphotonics-related industrial projects with companies, such as Barco, Agfa-Gevaert, Tyco, and Umicore. He has authored over 190 SCI-stated journal papers and over 400 publications in international conference proceedings. He edited 15 conference proceedings, authored seven chapters in books, and is a co-inventor of 15 patents. He was a Guest Editor of several special issues on Optical Interconnects for Applied Optics and the IEEE Journal of Selected Topics in Quantum Electronics. He is the General Chair of the International Society for Optical Engineers (SPIE) Photonics Europe conferences in Strasbourg and Brussels. He was a recipient of the International Commission for Optics Prize and the Ernst Abbe Medal from Carl Zeiss in 1999, and the IEEE Laser and Electro Optics Societys Distinguished Lecturer Award in 2003. Prof. Thienpont was also a recipient of the SPIE Presidents Award in 2005 for dedicated service to the European Community and the International Micro Optics Conference Award in 2007. He was an Invited Speaker at 50 international conferences. He is a fellow of SPIE and the European Optical Society, and a member of the Optical Society of America and the IEEE Lasers and Electro-Optics Society. He currently serves on the Board of Directors of SPIE, and is a member of the Board of Stakeholders of the Technology Platform Photonics21, a high-level advisory board for optics and photonics in EC FP 7.

PLACE PHOTO HERE

Krassimir Panajotov (M08) received the B.S., Ph.D., and D.Sc. degrees in physics from Sofia University, Sofia, Bulgaria, in 1982, 1988, and 2002, respectively. Since 1982, he has been appointed at the Institute of Solid State Physics (ISSP), Bulgarian Academy of Sciences, Sofia. Since 2001, he has led the Micro and Nano Photonics Group at ISSP. During 1996-1998, he was a Guest Researcher at the Vrije Universiteit Brussels, Brussels, Belgium, which he joined again in 2000. His research activities are in nonlinear optics, semiconductor lasers, photonic crystal devices, and nonlinear semiconductor laser dynamics. In these fields, he holds more than 170 SCI-stated journal papers, more than 180 publications in international conference proceedings, and 7 book chapters. He has led a number of projects on national level in Bulgaria and Belgium and international bilateral projects, and served as a National Coordinator of several European COST actions. He co-chaired the conferences on Semiconductor Laser and Laser Dynamics at the Photonics Europe2008,-2016, and five international workshops. He has served as a Guest Editor of four Special Issues of Optical and Quantum Electronics and Advances in Optics Technologies, as well as of 5 International Society for Optical Engineers proceedings. He is currently an Associate Editor of the Journal of Opto-Electronics Review. He is a member of IEEE and a Senior Member of the Optical Society of America.